

# Deterministic and stochastic aspects of VEGF-A production and the cooperative behavior of tumoral cell colony

Pasquale Laise<sup>a,d</sup>, Francesca Di Patti<sup>e</sup>, Duccio Fanelli<sup>b</sup>, Marika Masselli<sup>c</sup>,  
Annarosa Arcangeli<sup>c</sup>

<sup>a</sup>*CSDC Centro Interdipartimentale per lo Studio di Dinamiche Complesse, University of Florence, Italy and INFN*

<sup>b</sup>*Dipartimento di Energetica, University of Florence, Via S. Marta 3, 50139 Florence, Italy*

<sup>c</sup>*Dipartimento di Patologia e Oncologia Sperimentali, University of Florence, viale Morgagni 50, 50134 Florence, Italy*

<sup>d</sup>*INFN - Sezione di Firenze*

<sup>e</sup>*Dipartimento di Fisica G. Galilei, Università degli Studi di Padova, via Marzolo 8, 35131 Padova, Italy*

---

## Abstract

A model is proposed to study the process of hypoxia-induced angiogenesis in cancer cells. The model accounts for the role played by the vascular endothelial growth factor (VEGF)-A in regulating the oxygen intake. VEGF-A is dynamically controlled by the HIF-1 $\alpha$  concentration. If not degraded, HIF-1 $\alpha$  can bind to the subunit termed HIF-1 $\beta$  and so experience translocation to the nucleus, to exert its proper transcriptional activity. The delicate balance between these opposing tendencies translates into the emergence of distinct macroscopic behaviors in terms of the associated molecular concentrations that we here trace back to normoxia, hypoxia and death regimes. These aspects are firstly analyzed with reference to the ideal mean-field scenario. Stochastic fluctuations are also briefly discussed and shown to seed a cooperative interaction among cellular units, competing for the same oxygen reservoir.

*Keywords:* stochastic model, cancer, hypoxia, angiogenesis

*PACS:* 02.50.Ey, 05.40.-a, 82.20.Uv

---

## 1. Introduction

Hypoxia ( $O_2$  tension below 2.5 mmHg) is a hallmark of several types of solid tumor [11]. Growing clinical evidence postulates a correlation between hypoxia and cancer aggressiveness and metastasis [7]. Hypoxia may underlie resistance to radiotherapy and can modify the cancer phenotype through gene regulation. A major cellular response to hypoxia is the stabilization of hypoxia inducible factor 1 (HIF-1), a transcription factor that controls cancer progression, and represents a potential target for therapy [10]. HIF-1 is a heterodimer composed

of a oxygen-dependent HIF-1 $\alpha$  and a constitutively expressed subunit termed HIF-1 $\beta$ . The transcriptional response to HIF-1  $\alpha$  varies from general effects, such as the up regulation of anaerobic respiration (virtually in all tumors), to the more tissue-specific effects such as angiogenesis [11]. The tumor-driven angiogenesis is therefore a process pivotal in tumor growth and progression, and is mainly related to the HIF-1 dependent secretion of the angiogenic factor Vascular Endothelial Growth Factor -A (VEGF-A) [13]. Low  $O_2$  tension may shape the cancer phenotype. According to a recently proposed model for cancer progression [4], the tumor milieu exerts Darwinian selection in favor of cancer cells. The basis for this selection can be two-fold: firstly, the milieu may activate tumor-specific pathways. A second basis for selection may reside in the ability of cells to protect the intracellular compartment from a hypoxic milieu. Given the important role of hypoxia in cancer progression [4], targeting the cellular responses to hypoxia, including the triggering of VEGF-A secretion and the ensuing angiogenesis, may form an alternative to, or a component of, the current chemotherapeutical practice.

In this paper, a model is proposed to resolve the complex dynamical interplay between the molecular chemical species that participate to the aforementioned process. In particular, we will start by exploring the mean-field scenario stemming from the hypothesized networks of interaction. This formally amounts to operate in the limit for infinite system size, the species concentrations obeying to a closed set of ordinary differential equations. We target our analysis to the asymptotic (equilibrium) regime highlighting the emergence of different attractive (stable) states of the single cell dynamics, which appear to be selectively chosen depending on the chemical parameters involved. We then turn to consider the evolution of three neighbors cells which are effectively coupled via the external environment, and adjust consequently their interior dynamics. The role of fluctuations stemming from the discreteness of the system under scrutiny, is shortly addressed resorting to direct stochastic simulations. Depending on the selected parameters, normoxic condition can develop as an emergent dynamical equilibrium. Allowing for punctual mutations, so to mimic tumor derive, can alter the stability of the system, and eventually result in a competition between distinct cell populations. Indeed, as we shall demonstrate, cooperative mechanisms arise being mediated by the stochastic component of the dynamics. Interestingly, adjacent cells can also profit from the gained ability of an individual cell unit to survive under hypoxic condition, an effect which fades off in the continuum limit.

The paper is organized as follows. Next section is devoted to introducing the key ingredients of the model, here formulated as an ensemble of chemical equations. Then the mean-field version of the model is studied, which in turn corresponds to work in the infinite system size limit. The focus is on a single cell: different dynamical regimes are identified corresponding to distinct choices of the chemical parameters. Stochastic simulations are also performed to test the adequacy of the theory predictions and challenge *in silico* the role played by finite size corrections. Then in Sec. 5 we turn to discussing a generalization of the proposed model where three cells are made to interact and compete for the

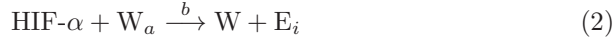
oxygen amount. Finally, in Sec. 6, we sum up and draw our conclusions.

## 2. A chemical model of hypoxia

Consider now an individual cell and assume the membrane barrier to divide between interior and exterior regions. Selected molecules can migrate through the semi-permeable membrane, being hence transported from the outside to the inside and viceversa. Aiming at elaborating a sound description of the hypoxia cycle [13], we select a set of candidate molecules which define a close ensemble of interacting elements, according to our schematic representation of the phenomenon under scrutiny. Oxygen molecules ( $O_2$ ) populate the external milieu. They diffuse and eventually reach the membrane where they happen to combine with the hydroxylases ( $W$ ), which are consequently turned into an active phase, hereafter labeled  $W_a$ <sup>1</sup>. This process is encapsulated into the following chemical equation:

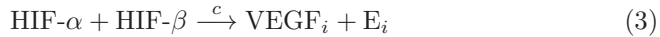


where  $a$  is the reaction rate and  $E_0$  stands for the empty case which the oxygen leaves behind when it gets absorbed by the  $W$ . The label 0 refers to the chemicals which are populating the outside region, while the molecules confined inside the cell wall are targeted with the subscript  $i$ . By introducing the concept of empty spaces ( $E_0$  outside, and  $E_i$  inside) we impose that the total number of elements (including the empties) is a constant of the dynamics [9, 2]. Active hydroxylases  $W_a$  interfere with the HIF- $\alpha$ , yielding to the degradation via the proteasome pathway:



Once the HIF- $\alpha$  is being targeted to degradation, the hydroxylases go back to the primitive configuration, waiting for the next oxygen to drive the transition into its active state. The degraded HIF- $\alpha$  molecule is replaced by the empty inner element  $E_i$ .

Moreover, the HIF- $\alpha$  can occasionally meet the HIF- $\beta$  subunit. This encounter necessarily takes place within the cell and gives rise to the VEGF <sub>$i$</sub>  macromolecule<sup>2</sup>. The corresponding chemical equation reads:

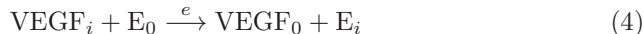


VEGF <sub>$i$</sub>  can eventually abandon the cell interior to occupy an external vacancy  $E_0$ , which is hence mutated into a VEGF<sub>0</sub> element. In formulae:

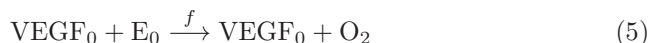
---

<sup>1</sup>Hydroxylases are intracellular enzymes, organized in three families respectively PHD1, PHD2, PHD3. Hydroxylases hence populate the internal flow and eventually combine with the oxygen that have penetrated the cell. As formalized in the following, we shall here focus on a more simple picture, and imagine that the encounters between hydroxylases and oxygen occur at cell boundary. In such a way, hydroxylases can be ideally pictured as antennae, localized on the membrane wall, chasing for the (outer) oxygen molecules.

<sup>2</sup>From hereon we will simply refer to VEGF-A as to VEGF.



Furthermore, the  $\text{VEGF}_0$  participates to the network of extracellular reactions which underlay the angiogenesis process. In practice, following a complex cascade of nested chemical reactions, the  $\text{VEGF}_0$  attracts the oxygen  $\text{O}_2$ , which is hence imagined to replace an (external) empty case. This materializes in turn into a simplified vision of a complex dynamic pathway, which has the sole scope of providing a self-consistent entry to the inspected process. The corresponding chemical equation takes the form:



Notice that the  $\text{VEGF}_0$  molecule is also a product of the reaction, a working hypothesis that we motivate with the empirical observation that  $\text{VEGF}_0$  can attract several oxygen units. This process will eventually come to a stop, as follows VEGF degradation which occurs both inside and outside the cells:



Finally, we should also account for the constitutive generation of HIF- $\alpha$  and HIF- $\beta$ :



The scenario outlined above is depicted in Fig. 1, where the main molecular actors are also specified<sup>3</sup>. It should be noted that the above model conserves the number of molecules which totals in  $N$ , a fact that is ultimately related to the presence of the empties species  $E$ .

We should emphasize that the proposed model is intimately stochastic, in its original chemical formulation. The inherent stochasticity emerges as an effect of the discreteness of the medium: finite size corrections, also termed demographic noise, result in a endogenous perturbation which can significantly impact the dynamics of the system as compared to the idealized continuum picture, which formally applies in the limit of infinite constituents. To respect the stochastic nature of the problem and simulate it in silico, one can resort to the celebrated Gillespie algorithm [6], a method which makes it possible to *exactly* monitor the time evolution of the *discrete* population of mutually interacting entities. The

---

<sup>3</sup>Importantly, the oxygen is initially imagined to fill the external reservoir, and solely re-integrated via the VEGF pathway. This is clearly a simplifying assumption, as in general one should also account for the oxygen supply via blood flux. On the other hand, we are here interested in the ability of the cell to self-organize when exposed to stressing condition, as it is the lack of oxygen income, a working hypothesis which justifies the assumed scenario.

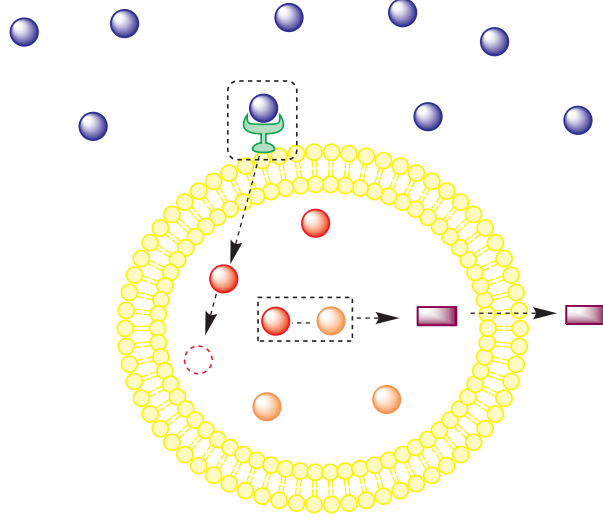


Figure 1: Cartoon for a single cell dynamics as follows the proposed scheme. Oxygen molecules (circles laying outside the cell) are captured by the hydroxylases sitting on the membrane, and so trigger the HIF- $\alpha$  (dark circles, red online, stored inside the membrane) elimination pathways (dashed circle). At the same time, HIF- $\alpha$  can combine with HIF- $\beta$  (light circles, orange online, stored inside the membrane), yielding to the (barrel like, in the picture) VEGF $_i$ . This latter can exit the cell wall, so ensuing in VEGF $_0$  and drive the incoming oxygen flux.

scheme captures in fact the probabilistic nature of the microscopic couplings and enables one to resolve the contribution associated to finite size fluctuations. As we shall demonstrate, stochastic fluctuations can eventually materialize in complex dynamics, which call for sound biological interpretation.

As anticipated, and opposed to the probabilistic approach, one can invoke the deterministic approximation, which in turn corresponds to assuming an infinite population amount and consequently disregarding finite size correlations. This defines the mean-field, continuum level of description, to which next sections are entirely devoted. More specifically, we will start by considering the case of a single cell, which we will discuss with reference to its mean field analogue. Notice that the deterministic formulation results from a straightforward derivation, that moves from the underlying master equation for the stochastic process, as defined by the above set of chemical equations. In the following, we will allude to such procedure, recalling its general philosophy, and just provide the end result for the case under inspection, without insisting on the technicalities. Working within the continuum representation we will then elaborate on the asymptotic dynamics of the recovered system of ordinary differential equations, by identifying distinct fixed points and discussing their associated stability characteristics. The inherent stochastic effects stemming from finite  $N$  corrections, will be relegated to section 5.

### 3. Master equation

At time  $t$ , the status of the chemical system, as ruled by the above reactions, is completely specified once the species amount are assigned. These are discrete entries, one for each species belonging to the ensemble of interacting population, which define the scalar components of the status vector  $\mathbf{n}$ . Recall that the system is intrinsically stochastic, its evolution being a suite of events which realizes with a prescribed probability. In mathematical terms, this fact implies dealing with the probability that the system is seen in the state  $\mathbf{n}$  at time  $t$ , hereafter denoted  $P(\mathbf{n}, t)$ . This latter quantity adjusts in time and obeys to the master equation:

$$\frac{d}{dt}P(\mathbf{n}, t) = \sum_{\mathbf{n}'} [T(\mathbf{n}|\mathbf{n}')P(\mathbf{n}', t) - T(\mathbf{n}'|\mathbf{n})P(\mathbf{n}, t)] \quad (10)$$

where  $T(\mathbf{n}'|\mathbf{n})$  denotes the transition rates between two adjacent states, from  $\mathbf{n}$  to  $\mathbf{n}'$ , compatible with the chemical constraints imposed by equations (1)-(9). For the sake of compactness, we omit here to list the specific forms of the transition rates relative to the model under analysis.

The partial differential equation (10) is an exact formulation, which can be in principle analyzed to track the system dynamics. In practice however, it is hard to analytically handle and further progress has to rely on direct numerical investigations.

The Gillespie algorithm represents in particular a viable strategy to simulate the time evolution of the probability distribution  $P(\mathbf{n}, t)$ . The method sets up a Monte Carlo procedure to determine the next reaction that is selected to occur, among all possible ones, and the time  $\tau$ , when the event takes place. Both selections reflect the assigned transition probabilities, which scales proportional to the number of substrate molecules times the associated reaction constants. Then, based on the selected reaction, the update of the molecule count follows, and time  $t$  is replaced by its value increased by the stochastic time interval  $\tau$ , namely  $t \rightarrow t + \tau$ .

Alternatively, the master equation (10) can be studied via perturbative methods, aimed at extracting both the idealized continuum picture and the successive finite size corrections. The van Kampen large  $N$  expansion is in this respect a widely adopted technique, extensively characterized in the literature [5, 12]. In the following section, we shall operate within the van Kampen framework to derive a closed system of ordinary differential equations for the coupled evolution of the concentrations of chemical system (1)-(9) in the limit of large (formally infinite)  $N$ .

### 4. Mean-field solution of the single cell model

Let us focus on a single cell, as pictorially represented in Fig. 1. Consider for instance the  $\text{O}_2$  species. According to van Kampen [12], one can put forward

the following ansatz for the associated mean-field (continuous) concentration here labeled  $\mathcal{O}$ :

$$\mathcal{O} = \frac{n_{O_2}}{N} + \frac{\xi}{\sqrt{N}}$$

where the extensive quantity  $n_{O_2}$  is discrete: it is one of the components of the vector  $\mathbf{n}$  and stands for the number of oxygen molecules.  $\xi$  is instead a stochastic variable and contributes with an additive terms which scales as  $1/\sqrt{N}$ , so materializing in a perturbation to the idealized mean-field dynamics. Stochastic effects can be hence safely neglected when performing the continuum limit [5, 12], the relic concentration obeying to a deterministic set of coupled differential equations. We recall however that beyond the idealized scenario, finite size corrections do matter when real systems are concerned, the intimate discreteness being a crucial ingredient of the dynamics. We shall return on this issue in Section 5, to highlight the important impact of such an endogenous source of stochastic perturbation with reference to the scrutinized model.

For simplicity, by extending the above reasoning to the other involved species, we will here denote by  $\mathcal{W}$ ,  $\mathcal{W}_a$ ,  $\mathcal{V}_0$ ,  $\mathcal{V}_i$ ,  $\mathcal{E}_0$ ,  $\mathcal{E}_i$ ,  $\mathcal{H}_\alpha$  and  $\mathcal{H}_\beta$  the average (mean-field) concentration of W,  $W_a$ , VEGF<sub>0</sub>, VEGF<sub>*i*</sub>, E<sub>0</sub>, E<sub>*i*</sub>, HIF- $\alpha$  and HIF- $\beta$  respectively. According to this notation, the mean-field equations take the form<sup>4</sup>:

$$\frac{d}{dt}\mathcal{O} = -a\mathcal{O}\mathcal{W} + f\mathcal{V}_0\mathcal{E}_0 \quad (11)$$

$$\frac{d}{dt}\mathcal{W} = -a\mathcal{O}\mathcal{W} + b\mathcal{W}_a\mathcal{H}_\alpha \quad (12)$$

$$\frac{d}{dt}\mathcal{W}_a = a\mathcal{O}\mathcal{W} - b\mathcal{W}_a\mathcal{H}_\alpha \quad (13)$$

$$\frac{d}{dt}\mathcal{H}_\alpha = -b\mathcal{W}_a\mathcal{H}_\alpha - c\mathcal{H}_\alpha\mathcal{H}_\beta + g_\alpha\mathcal{E}_i \quad (14)$$

$$\frac{d}{dt}\mathcal{H}_\beta = -c\mathcal{H}_\alpha\mathcal{H}_\beta + g_\beta\mathcal{E}_i \quad (15)$$

$$\frac{d}{dt}\mathcal{V}_i = c\mathcal{H}_\alpha\mathcal{H}_\beta - e\mathcal{V}_i\mathcal{E}_0 - d\mathcal{V}_i \quad (16)$$

$$\frac{d}{dt}\mathcal{V}_0 = e\mathcal{V}_i\mathcal{E}_0 - d\mathcal{V}_0 \quad (17)$$

$$\frac{d}{dt}\mathcal{E}_i = b\mathcal{W}_a\mathcal{H}_\alpha + c\mathcal{H}_\alpha\mathcal{H}_\beta + e\mathcal{E}_0\mathcal{V}_i + d\mathcal{V}_i - (g_\alpha + g_\beta)\mathcal{E}_i \quad (18)$$

with the conservation law

$$\mathcal{O} + \mathcal{W} + \mathcal{V}_0 + \mathcal{V}_i + \mathcal{E}_0 + \mathcal{W}_a + \mathcal{E}_i + \mathcal{H}_\alpha + \mathcal{H}_\beta = 1 \quad (19)$$

---

<sup>4</sup>In deriving eqs. (18) correlations have been neglected, a legitimate choice in the mean-field approximation and whose validity has been tested versus numerical simulation in a number of models that follow the same conceptual scheme [8, 3].

Notice that the same result could be recovered without the use of the van Kampen's expansion. Indeed, multiplying both sides of the master equation by a scalar component of the status vector  $\mathbf{n}$ , summing over all  $\mathbf{n}$ , shifting some of the involved sums by  $\pm 1$  and neglecting the correlations (which is legitimate in the  $N$  infinite limit) one recovers the same mean field system.

From Eq. (12) and (13), it straightforwardly follows that  $\mathcal{W}_a + \mathcal{W}$  stays constant: This invariant quantity is hereafter set equal to  $n_0$  and specified by the initial condition. To investigate the dynamics of the above system (11) - (18), and in particular elaborate on its asymptotic evolution, one can look for stationary solutions. These are the fixed points of the dynamics, which can be explicitly found by setting to zero the derivatives in (11) - (18) and solving the obtained algebraic system, where the (final) concentration amounts enter as unknowns.

#### 4.1. Stationary states

Solving for the fixed points returns three possible solutions. These latter are here characterized and labeled via the progressive indexes  $i = 1, 2, 3$ , associated to the predicted asymptotic concentrations. Two solutions can be readily obtained via direct inspection of the above equations, and correspond to opposite tendencies that we will hereafter call *normoxia* and *death* respectively.

Normoxia conditions are assumed to correspond to the asymptotic solution:

$$\mathcal{V}_{0,1} = \mathcal{V}_{i,1} = \mathcal{H}_{\alpha,1} = \mathcal{W}_1 = \mathcal{E}_{i,1} = 0. \quad (20)$$

HIF- $\alpha$  is turned off and so are the inner/outer concentrations of VEGF. The HIF- $\alpha$  degradation mechanism hence prevails over the alternative pathway that yields VEGF production, and which could in principle contribute to enhance the oxygen supply. The amount of  $\text{O}_2$ , here quantified by  $\mathcal{O}_1$ , is on the contrary sufficient to guarantee the correct cell functioning. Hydroxylases are frozen in their active state  $\mathcal{W}_a$  and consequently stimulate the repression of the HIF- $\alpha$  quota<sup>5</sup>. From the conservation relations we immediately deduce the following relation:

$$\mathcal{W}_{a,1} = n_0 \quad (21)$$

$$\mathcal{O}_1 + \mathcal{E}_{0,1} + \mathcal{H}_{\beta,1} = 1 - n_0 \quad (22)$$

The outer cases are shared between oxygen and empties, as exemplified by the latter equation, in a proportion that cannot be predicted a priori.

---

<sup>5</sup>In the transient dynamics, HIF- $\alpha$  molecules are indeed present and translate into VEGF entities, upon combination with HIF- $\beta$ . VEGF molecules can remain temporarily active also when the HIF- $\alpha$  has been eliminated, and so drive a consequent oxygen influx. There is hence a certain degree of inertia which increments the initial oxygen amount. The effect becomes more pronounced as  $g_\alpha$  gets larger, more HIF- $\alpha$  populating the cell during the transient dynamics, before degradation has occurred. However, provided  $g_\alpha$  is small enough, the cell reaches a steady state configuration, with no residual amount of HIF- $\alpha$  molecules. For this reason, we refer to this configuration as to the normoxia regime.



As opposed to normoxia condition, a trivial solution of the mean field problem is found when:

$$\mathcal{W}_{a,3} = \mathcal{V}_{0,3} = \mathcal{V}_{i,3} = \mathcal{H}_{\alpha,3} = \mathcal{E}_{i,3} = \mathcal{O}_3 = 0 \quad (23)$$

with in addition  $\mathcal{W}_3 = n_0$  and  $\mathcal{E}_{0,3} + \mathcal{H}_{\beta,3} = 1 - n_0$ . In this case, the cell is dead: the oxygen amount is zero and the hydroxylases cycle is not active, so denouncing the lethargic state of the cell device.

An intermediate asymptotic stationary state is also possible, when the cell balances the oxygen consumption by properly adjusting the VEGF production cycle, at equilibrium. Upon manipulation of the fixed point equations associated to the system (11) - (18), the equilibrium solution for  $\mathcal{E}_{0,2}$  is found to verify the following quadratic equation:

$$\frac{fe}{d}\mathcal{E}_{0,2}^2 - \left(\frac{g_\alpha}{g_\beta} - 1\right)d\mathcal{E}_{0,2} - d\left(\frac{g_\alpha}{g_\beta} - 1\right) = 0 \quad (24)$$

The previous equation admits a solution only if  $g_\alpha > g_\beta$ , otherwise is reduced to a sum of three positive terms which cannot mutually cancel for positive coefficients and state variables. When  $g_\alpha = g_\beta$ , then  $\mathcal{E}_{0,2} = 0$ , which corresponds to having the largest allowed oxygen concentration  $\mathcal{O}_2 = 1 - n_0$ . This latter can alternatively be seen as a limiting normoxia condition. All externally available cases are simultaneously occupied by oxygen molecules, which can still effectively contrast the HIF- $\alpha$  generation, while providing the necessary supply for the cell functioning ( $\mathcal{W}_{a,1} \neq 0$ ). Beyond this condition, a quota of HIF- $\alpha$  survives the degradation and sustains the VEGF production process. VEGF molecules transported outside the cell support the afflux of oxygen and so contribute to stabilize the quota of HIF- $\alpha$ . In practical terms, the condition  $g_\alpha = g_\beta$  (when the HIF- $\alpha$  and HIF- $\beta$  production rates equalize) signals a transition between two distinct asymptotic regimes, a fact that could be further appreciated by quantifying the values assumed by the remaining involved concentrations. We identify the intermediate fixed point with the *hypoxia* conditions: The cell is in fact alive thanks to a dedicated feedback that integrates the original oxygen amount via the VEGF production. Once  $g_\alpha > g_\beta$  the solution of Eq. (24) reads:

$$\mathcal{E}_{0,2} = \frac{d \left[ e(g_\alpha - g_\beta) + \sqrt{e(g_\alpha - g_\beta) [e(g_\alpha - g_\beta) + 4fg_\beta]} \right]}{2feg_\beta} \quad (25)$$

The equilibrium values of the other variables cannot be univocally determined. However, given the value of  $\mathcal{E}_{0,2}$  as estimated above, the following ratios

are fixed:

$$\begin{aligned}
\frac{\mathcal{O}_2 \mathcal{W}_2}{\mathcal{V}_{0,2}} &= \frac{f}{a} \mathcal{E}_{0,2} \\
\frac{\mathcal{W}_{a,2} \mathcal{H}_{\alpha,2}}{\mathcal{V}_{0,2}} &= \frac{f}{b} \mathcal{E}_{0,2} \\
\frac{\mathcal{H}_{\alpha,2} \mathcal{H}_{\beta,2}}{\mathcal{V}_{0,2}} &= \frac{g_\beta}{c} \frac{f}{g_\alpha - g_\beta} \mathcal{E}_{0,2} \\
\frac{\mathcal{E}_{i,2}}{\mathcal{V}_{0,2}} &= \frac{f}{g_\alpha - g_\beta} \mathcal{E}_{0,2} \\
\frac{\mathcal{V}_{i,2}}{\mathcal{V}_{0,2}} &= \frac{d}{e} \frac{1}{\mathcal{E}_{0,2}}
\end{aligned}$$

Notice that an implicit relation between  $\mathcal{W}_{a,2}$  and  $\mathcal{V}_{0,2}$  is also derived by making use of Eq. (19). More interestingly, for the case  $g_\alpha > g_\beta$ ,  $\mathcal{E}_{0,2}$  can be shown to increase with  $g_\alpha$ , while keeping all the other parameters constant. The maximum value that can be eventually attained is  $\mathcal{E}_{0,max} = 1 - n_0$ , a limiting condition that, together with  $g_\alpha > g_\beta$ , identifies the portion of parameters plane for which the hypoxia fixed point do exist. More specifically, the largest the values of  $f$ , i.e. the rate of oxygen production via the VEGF cycle, the wider the window in  $g_\alpha$  that delimits the hypoxia regime. Working in the  $(g_\alpha, f)$  plane we can analytically determine the boundaries of the domain of existence of the non trivial fixed point. Its equation can be deduced by imposing  $\mathcal{E}_{0,2} = \mathcal{E}_{0,max}$  into Eq. (24) which immediately yields to

$$f = \frac{ed\mathcal{E}_{0,max} + d^2}{g_\beta e \mathcal{E}_{0,max}^2} g_\alpha - \frac{ed\mathcal{E}_{0,max} + d^2}{e \mathcal{E}_{0,max}^2}$$

This is a line which crosses the axis  $f = 0$  when  $g_\alpha = g_\beta$ , see Fig. 2 where three domains, respectively I, II, III, are outlined. Notice that the normoxia and death solutions can in principle extend over all the parameters plane, while the hypoxia is solely bound to region II. The hypoxia region shrinks as  $f$  is reduced and eventually fades off when the VEGF's ability to carry oxygen is hindered. We recall in fact that within our simplified formulation, the oxygen income is ultimately controlled by the parameter  $f$ , and consequently linked to the available VEGF<sub>0</sub> quota. It is hence plausible that that region here identified to correspond to the hypoxia regime vanishes when  $f$  is set to zero. Numerical simulations indicate that the basin of attraction of the normoxia state prevails in region I, while the death configuration dynamically takes over in region III. In region II, it is the hypoxia condition to represent the stable attractor of the dynamics. For this reason, region I, II and III are respectively termed normoxia, hypoxia and death, and the caption of Fig. 2 reflects such a choice. To gain further insight into this empirical observation, we turn in the next section to studying the stability properties of the identified fixed point. The analysis is carried out via combined numerical and analytical means, as the complexity of the model prevents us from performing a complete analytical treatment.

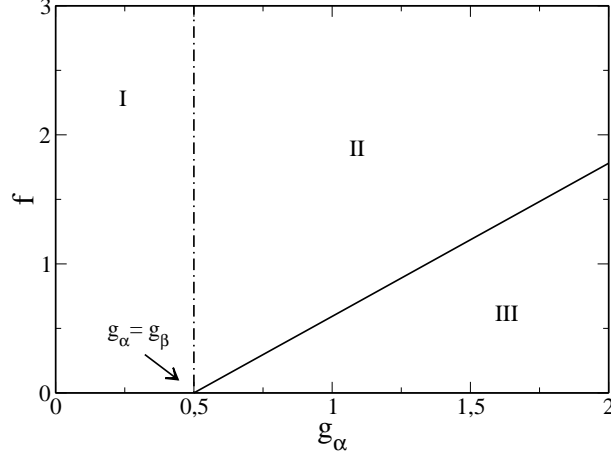


Figure 2: The existence of the normoxia (I), hypoxia (II) and death (III) regions is displayed in the  $(g_\alpha, f)$  plane, as predicted by the mean-field calculations for  $N = 1000$ ,  $n_0 = 20$ ,  $e = 0.9$ ,  $d = 0.4$  and  $g_\beta = 0.5$ . The transition from I to II is found to occur when  $g_\alpha = g_\beta$ , i.e. when the HIF- $\alpha$  production rate prevails over the HIF- $\beta$  one. Then the exceeding HIF- $\alpha$  is stabilized to an asymptotic fixed concentration via the additional VEGF pathway. It can be further appreciated that region II gets compressed when reducing the control parameter  $f$ .

#### 4.2. Stability analysis

In this section we set down to study the stability properties of the three families of equilibrium points, as identified above. To this end we calculate the Jacobian matrix associated to the system (11)-(18), explicitly given in the Appendix and evaluate the eigenvalues relative to the three fixed points, namely the normoxia, the hypoxia and the death.

Consider first the solution that corresponds to the cellular death, previously labeled with the index 3 in the concentration. We recall that  $\mathcal{W}_{a,3} = \mathcal{V}_{0,3} = \mathcal{V}_{i,3} = \mathcal{H}_{\alpha,3} = \mathcal{E}_{i,3} = \mathcal{O}_3 = 0$ ,  $\mathcal{W}_3 = n_0$ , while the concentration  $\mathcal{E}_{0,3}$  and  $\mathcal{H}_{\beta,3}$  can in principle take any value, constrained by the relation  $\mathcal{E}_{0,3} + \mathcal{H}_{\beta,3} = 1 - n_0$ , which ultimately specifies the family of possible solutions. The associated characteristic polynomial reads:

$$\lambda^3(\lambda + an_0)(\lambda + d) \det \begin{pmatrix} \lambda + c\mathcal{H}_{\beta,3} & 0 & -g_\alpha \\ -c\mathcal{H}_{\beta,3} & \lambda + e\mathcal{E}_{0,3} + d & 0 \\ -c\mathcal{H}_{\beta,3} & -e\mathcal{E}_{0,3} - d & \lambda + g_\alpha + g_\beta \end{pmatrix} = 0 \quad (26)$$

where  $\lambda$  stands for the eigenvalue. It is evident that  $\lambda_1 = \lambda_2 = \lambda_3 = 0$ ,  $\lambda_4 = -an_0$  and  $\lambda_5 = -d$  are possible solution of Eq. (26). The remaining three eigenvalues cannot be analytically determined. For  $g_\alpha > g_\beta$  (a condition that embraces region II and III of the parameters plane depicted in Fig. 2), analytical progress is possible: just one stable solution exists among those of type 3 that are in principle admissible. To substantiate this observation, let us

denote with  $J_3^{sub}$  the non trivial sub-matrix of the full Jacobian (26):

$$J_3^{sub} = \begin{pmatrix} -c\mathcal{H}_{\beta,3} & 0 & +g_\alpha \\ +c\mathcal{H}_{\beta,3} & -e\mathcal{E}_{0,3} - d & 0 \\ +c\mathcal{H}_{\beta,3} & +e\mathcal{E}_{0,3} + d & -g_\alpha - g_\beta \end{pmatrix}.$$

It is easy to see that  $\det(J_3^{sub}) = c\mathcal{H}_\beta(g_\alpha - g_\beta)(d + e\mathcal{E}_{0,3})$ , and so  $\det(J_3^{sub}) > 0$   $\forall \mathcal{H}_{\beta,3} > 0$  and  $g_\alpha > g_\beta$ . Positive determinant implies unstable solutions, as can be immediately appreciated with simple algebraic considerations. This means that the fixed point corresponding to the death state is always unstable when  $g_\alpha > g_\beta$ , and  $\mathcal{H}_{\beta,3} \neq 0$ , this latter quantity being positively defined. At variance, stable solution can manifest in the region specified by condition  $g_\alpha > g_\beta$ , when  $\mathcal{H}_{\beta,3} = 0$ . This latter request equivalently implies  $\mathcal{E}_{0,3} = 1 - n_0$ , and removes the degeneracy (at least in region I and II) by uniquely characterizing the fixed point of type III selected by the dynamics. The only stable fixed point of type “death” in region II and III, is now completely specified and the three lacking eigenvalues can be readily calculated, resulting in  $\lambda_6 = 0$ ,  $\lambda_7 = -e(1 - n_0) - d$  and  $\lambda_8 = -g_\alpha - g_\beta$ . Solutions of type 3 are clearly stable also in region I, suggesting that the cell can always meet the conditions that drive its death, an asymptotic fate which is ultimately determined by the selected initial datum (corresponding to the environmental conditions).

However, direct numerical inspection, suggests that within region II, the system tends to converge to the hypoxia solution, this latter being hence dynamically favored over the stable death regime. Tracing the respective basins of attraction can be tackled via a dedicated campaign of numerical simulations. Biologically, it can be hence speculated that for sufficiently large values of the parameter  $g_\alpha$  the cell opposes the death derive, by compressing its respective basin of attraction upon activation of the hypoxia cycle.

In region I, when  $g_\alpha < g_\beta$ , an infinite family of solutions of type 3 can in principle manifest, depending on the specific initial datum. The associated eigenvalues can be calculated numerically by tuning both  $\mathcal{H}_{\beta,3}$  and  $\mathcal{E}_{0,3}$  within the allowed range of variation, pointing to the stability of the solutions. Again, the cell can always die in response to particularly stressing conditions. To complete the description of region I, one needs to address the stability properties of the normoxia solution. In this case, repeating the above strategy, the characteristic polynomial turns out to be

$$\lambda^3(\lambda + a\mathcal{O}_1)(\lambda + d) \det \begin{pmatrix} \lambda + b\mathcal{W}_{a,1} + c\mathcal{H}_{\beta,1} & 0 & -g_\alpha \\ -c\mathcal{H}_{\beta,1} & \lambda + e\mathcal{E}_{0,1} + d & 0 \\ -b\mathcal{W}_{a,1} - c\mathcal{H}_{\beta,1} & -e\mathcal{E}_{0,1} - d & \lambda + g_\alpha + g_\beta \end{pmatrix} = 0$$

which immediately gives  $\lambda_1 = \lambda_2 = \lambda_3 = 0$ ,  $\lambda_4 = -a\mathcal{O}_1$  and  $\lambda_5 = -d$ . In this case the determinant of the residual  $3 \times 3$  sub-matrix does not return any sensible information on the sign of the real part of the three unknown eigenvalues. To overcome this limitation we proceed as follows: we first integrate numerically the governing system of differential equations and then select the attained equilibrium fixed point, as an entry to calculate the full set of eigenvalues. Among

the missing eigenvalues, two (which can be complex or real depending on  $g_\alpha$ ) always display a negative real part, while the third one is real and can change the sign as  $g_\alpha$  is increased. This situation is illustrated in the inset of Fig. 4: the real eigenvalue is negative over a range of parameters that practically corresponds to region I, and it approaches zero for  $g_\alpha \gtrsim g_\beta$ . This result holds true for different parameters choice (i.e. the value of  $f$ ) and selected initial conditions. It can hence be argued that the normoxia condition is stable within region I and that it gets unstable when the boundary of region II, the domain of existence of the hypoxia solution, is (continuously) approached. Indeed, within region I, the competition between the two attractors of type 1 (normoxia) and 3 (death) is dynamically resolved to favor the former, as confirmed by direct numerical inspection.

In conclusion, the proposed model can alternatively yield to three distinct dynamical regimes, depending on the specific choice of the chemical parameters. The normoxia condition is stable in region I and loses its stability when the edges of the domain II are approached. In this latter region it is the hypoxia solution to take over, by prevailing over the death regime which instead dominates in region III. Interestingly, death is always an attractive state of the dynamics, irrespectively of the selected parameters, a tendency that the cell efficiently opposes in region I and II. Formally, it is hence not accurate to talk about a transition among the three states, the landscape of possible stable attractors being more complex as outlined above. However, to keep the message simple, we shall hereafter reflect the practical segregation into three distinct zones, as virtual transitions. Notice that a punctual mutation of the reference parameters could substantially alter the cell functioning and determine its death. In the next subsection we turn to numerical simulations to validate the proposed scenario. The simulations here performed refer both to the idealized mean-field dynamics and to the stochastic scenario which respects the inherent discreteness of the chemical medium.

#### 4.3. Numerical simulations vs. mean field theory

In this section we report about a campaign of simulations aimed at validating the theoretical picture depicted above. Mean-field ordinary differential equations (11)-(18) can be straightforwardly integrated via a standard Runge-Kutta scheme. In Fig. 3 the time evolution of  $\text{VEGF}_i$  and active hydroxylases is reported (solid lines) for different values of the parameters. Panels (a) and (b) refer to a choice of the parameters that yield to the normoxia condition: Once the transient has died out, the system achieves its asymptotic state where VEGF molecules are absent. At variance,  $W_a$  attains its equilibrium concentration, different from zero. The same applies to oxygen (not displayed here). When increasing the parameter  $g_\alpha$ , which controls the HIF- $\alpha$  production rate, a transition occurs towards what we termed the hypoxia regime, see panels (c) and (d). Here the HIF- $\alpha$  quota is sensibly different from zero, implying the existence of a positive feedback reaction on the oxygen production, via the VEGF molecules. By further augmenting  $g_\alpha$ , one gradually approaches the boundary of the third allowed region, as previously outlined: When  $g_\alpha$  is large enough, all

chemical concentrations drop to zero, including the  $W_a$  amount, which is here assumed to signal the cell activity. This scenario is clearly displayed in panels (e) and (f) of Fig. 3.

Beside integrating the system of differential equations (11)-(18), one can turn to direct stochastic simulations, which enables one to treat the interacting molecules as diffusing massive entities, so respecting the finiteness of the chemical environment. To this end, we resort to the Gillespie algorithm: as already recalled, this is a sophisticated Monte Carlo scheme which enables to inspect the actual dynamics of an ensemble made of discrete actors, whose relative interactions are specified by an assigned set of chemical rules. The outcome of the stochastic integration is superposed in Fig. 3, to the curves determined within the mean-field approximation. The intrinsic stochastic noise materializes as a local disturbance of the reference mean-field profile, suggesting that the discreteness of the environment contributes modestly to the system dynamics. As opposed to this vision, we will prove in the following that finite size correction can be important and can eventually result in drastic modification of the dynamical behavior, as predicted within the mean-field scenario.

Before turning to analyze these aspects, we provide in Fig. 4 a global picture of the distinct dynamical regimes that can be faced when tuning the  $(f, g_\alpha)$  parameters: Here the asymptotic concentration of  $VEGF_i$ , as calculated upon integration of Eqs. (11) - (18) is plotted with a colorcode. The existence of three different regions, is clearly confirmed, the transition from normoxia (I) to hypoxia (II) being sharper and hence more evidently appreciated. As a further complement, we enclose a section of the scanned parameters plane, by reporting the recorded concentration of  $VEGF_i$  versus  $g_\alpha$ , at fixed  $f$ . The double transition is shown, bearing intriguing analogy with the phenomenon of re-entrant phase transitions.

## 5. Dynamics in a multicellular environment: Synchronization and cooperative effects

To shed light onto the cooperative effects that might eventually arise in a colony of interacting cell units, we here consider  $N_c = 3$  cells obeying to the chemical equations hypothesized above. Now the oxygen fills a shared reservoir, from which any individual cell can draw. The cells are hence mutually, though indirectly, communicating via the oxygen amount. A schematic layout of the interaction network is depicted in Fig. 5. In this case we need to introduce an extra label to specify the cell to which the molecules belong to. In practical terms, one is forced to deal with the molecules  $VEGF_i^j$ ,  $E_i^j$ ,  $HIF-\alpha^j$  and  $HIF-\beta^j$  with  $j = 1, \dots, N_c$ . The governing chemical equations follow as a straightforward generalization of Eqs. (1)-(9). The mean-field system calculated from the underlying master equation is now composed by  $4 \times N_c + 3$  equations (not explicitly given here), the coupling being indirectly provided by the species hosted in the outer environment which constitutes a shared reservoir.

Working within this generalized setting, interesting cooperative effects arise, as supported by the discrete component of the dynamics. In the finite  $N$  regime,

correlations exist between the evolving species and translate into important contributions that can affect the system dynamics. The correlations are instead neglected within the mean-field approximation, formally valid when the container is filled with an infinite amount of molecular constituents. To demonstrate the importance of finite size corrections, we assign to two cells a set of parameters (including the  $g_\alpha$  value) which is found to yield to the death condition, in the mean field regime and according to the preceding classification. The third cell is instead imagined to bear a  $g_\alpha$  parameter in the hypoxia domain (while keeping the other parameters unchanged), as identified above. What is going to happen to the considered system of three cells?

In Fig. 6 the evolution of hydroxylase is reported as a function of time. The solid lines (red online) stand for the mean-field dynamics, obtained by numerical integration of the generalized set of ordinary differential equations which accounts for the three inspected cells. Two cells are destined to die (no residual  $W_a$ ), while the third survives ( $W_a$  are eventually present). Interestingly the stochastic dynamics is peculiarly different, as displayed in Fig. 6 (wiggling curves, cyan online). As resulting from a cooperative mechanism, ultimately driven by the finiteness of the simulated medium, and so not captured within the corresponding continuous description, the two cells destined to death are rescued by the third cell. This latter can sustain the angiogenesis process and so integrate the oxygen quota which is necessary for the correct functioning of its nearest neighbors. The rescued cells do partially contribute by stimulating the production of VEGF. Synchronized oscillations are observed in the recorded dynamics of the active hydroxylases, as displayed in the zoomed inset of Fig. 6.

In conclusion, and based on the above findings, it is tempting to speculate that the observed degree of cooperation turns out particularly crucial for understanding the adaptation of tumoral cells in a changing environment. Under stressing condition, it is well known that tumoral cells can undergo mutation, changing their specific abilities and fully exploiting their inherent flexibility. Assume that under stressing condition the oxygen income is not enough to guarantee the cell functioning. Then the tumoral cells would undergo a critical phase, which could induce punctual mutations. In particular, imagine that following such random adjustments, a cell enters the regime of hypoxia (in our model, by properly tuning the corresponding  $g_\alpha$  parameter). This corresponds to reducing the HIF- $\alpha$  production rate, so consequently freeing a quota of oxygen, otherwise employed in the HIF- $\alpha$  degradation pathway. Therefore not only the tumoral cell interested by the mutation can survive, but also the cells populating the local neighborhood (which are plausibly also belonging to the tumoral family although not necessarily affected by the same mutation), follows a cooperative interaction. This effect is here reproduced within a sound dynamical picture where finite size effects prove to be crucial.

## 6. Conclusions

In this paper we have discussed a simplified model to quantitatively address the dynamical mechanisms which ultimately underlie the angiogenesis process.

The dynamical interplay between a limited number of molecular species is resolved and investigated both via numerical and analytical techniques. The level of complexity of the proposed description results from a trade-off balance between the request of incorporating a fair amount of biological information, and the need of making the problem analytically tractable. Within the proposed formulation, the cell can follow different routes, depending on the specific values of the involved chemical parameters. Distinct macroscopic regimes are here discussed and associated to normoxia, hypoxia and death conditions respectively. The rate of HIF- $\alpha$  production, as well as the parameter that controls the ability of VEGF to call for new oxygen, are shown to play a crucial role in determining the transition between the admissible dynamical regimes. These latter are analytically explained via a mean-field based calculation, which is fully confirmed by direct numerical simulations. The role of stochastic noise is also elucidated and shown to drive a degree of synchronization between the cells belonging to a given colony. This is a spontaneously emerging feature, stemming from the intimate discrete nature of the molecular environment, which can potentially relate to the attested adaptivity of localized families of tumoral cells. In fact, it is in general believed that cancer cells can react to the external stressing stimuli (as for the lack of oxygen) by favoring a specific mutation, which renders them more adaptable to the hosting environment. While this is a customarily evoked scenario, the simultaneous occurrence of the same mutation in all the cancer cell population appears a highly improbable event. Cooperative survival mechanisms, as those here identified, could in turn contribute to explain the observed robustness, via a self-consistent dynamical argument. As an additional point, the results of this paper can be of interest in studying the growth of a tumor cord characterized by an aerobic-anaerobic switch triggered by hypoxia [1].

## 7. Acknowledgments

The work was supported by grants from the Associazione Genitori contro le Leucemie e Tumori Infantili Noi per Voi, Associazione Italiana per la Ricerca sul Cancro, Istituto Toscano Tumori to AA, Ente Cassa di Risparmio di Firenze to the Dipartimento di Patologia e Oncologia Sperimentali, Università degli Studi di Firenze.

## Appendix A. Jacobian matrix

The Jacobian matrix associated to the system (11)-(18) reads

$$\mathbf{J} = \begin{pmatrix} -a\mathcal{W} & -a\mathcal{O} & 0 & 0 & 0 & 0 & f\mathcal{E}_0 & 0 \\ -a\mathcal{W} & -a\mathcal{O} & +b\mathcal{H}_\alpha & +b\mathcal{W}_a & 0 & 0 & 0 & 0 \\ +a\mathcal{W} & +a\mathcal{O} & -b\mathcal{H}_\alpha & -b\mathcal{W}_a & 0 & 0 & 0 & 0 \\ 0 & 0 & -b\mathcal{H}_\alpha & -b\mathcal{W}_a - c\mathcal{H}_\beta & -c\mathcal{H}_\alpha & 0 & 0 & g_\alpha \\ 0 & 0 & 0 & -c\mathcal{H}_\beta & -c\mathcal{H}_\alpha & 0 & 0 & g_\beta \\ 0 & 0 & 0 & +c\mathcal{H}_\beta & +c\mathcal{H}_\alpha & -e\mathcal{E}_0 - d & 0 & 0 \\ 0 & 0 & 0 & 0 & 0 & +e\mathcal{E}_0 & -d & 0 \\ 0 & 0 & b\mathcal{H}_\alpha & b\mathcal{W}_a + c\mathcal{H}_\beta & c\mathcal{H}_\alpha & e\mathcal{E}_0 + d & 0 & -g_\alpha - g_\beta \end{pmatrix}$$



## References

- [1] Astanin, S., Preziosi, L., 2009. Mathematical modelling of the warburg effect in tumour cords. *J. Theor. Biol.* 258, 578–590.
- [2] Dauxois, T., Di Patti, F., McKane, A., Fanelli, D., 2009. Enhanced stochastic oscillations in autocatalytic reactions. *Phys. Rev. E* 79, 036112.
- [3] Di Patti, F., Fanelli, D., 2009. Can a microscopic stochastic model explain the emergence of pain cycles in patients? *J. Stat. Mech.* 1, P01004.
- [4] Fang, J. S., Gillies, R. D., Gatenby, R. A., 2008. Adaptation to hypoxia and acidosis in carcinogenesis and tumor progression. *Seminars in cancer biology* 18, 330–337.
- [5] Gardiner, C. W., 1985. *Handbook of Stochastic Methods*, 2nd Edition. Springer.
- [6] Gillespie, D. T., 1976. A general method for numerically simulating the stochastic time evolution of coupled chemical reactions. *J. Comp. Phys.* 22, 403–434.
- [7] Koong, A. C., Mehta, V. K., Le, Q. T., Fisher, G. A., Terris, D. J., Brown, J. M., Bastidas, A. J., Vierra, M., 2000. Pancreatic tumors show high levels of hypoxia. *Int. J. Radiation Oncology Biol. Phys.* 48, 919–922.
- [8] McKane, A. J., Nagy, J. D., Newman, T. J., Stefanini, M. O., 2007. Amplified biochemical oscillations in cellular systems. *J. Stat. Phys.* 128, 165–191.
- [9] McKane, A. J., Newman, T. J., 2005. Predator-prey cycles from resonant amplification of demographic stochasticity. *Phys. Rev. Lett.* 94, 218102.
- [10] Semenza, G. L., 2003. Targeting HIF-1 for cancer therapy. *Nature reviews* 3, 721–732.
- [11] Tatum, J. L., Kelloff, G. J., Gillies, R. J., 2006. Hypoxia: importance in tumor biology, noninvasive measurement by imaging, and value of its measurement in the management of cancer therapy. *Int. J. Radiat. Biol.* 82, 699–757.
- [12] van Kampen, N. G., 1992. *Stochastic processes in Physics and Chemistry*. North Holland, Amsterdam.
- [13] Vaupel, P., 2004. The role of hypoxia-induced factors in tumor progression. *The Oncologist* 9, 10–17.

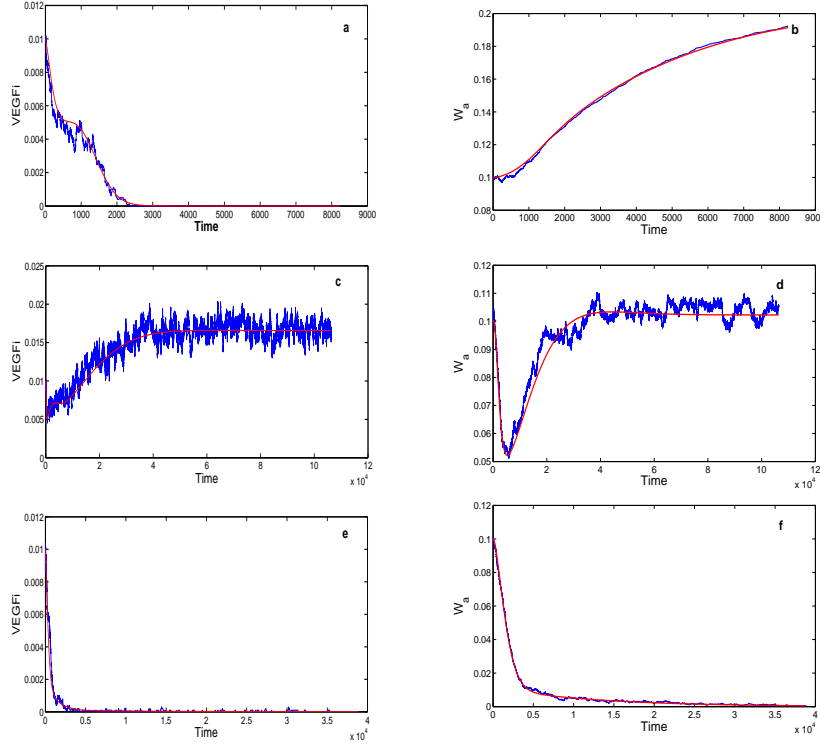


Figure 3: Simulated dynamics of system (11) - (18) for different choices of the chemical parameters. Panels (a) and (b) report the time evolution of the concentration of VEGF<sub>i</sub> and W<sub>a</sub> respectively, for  $a=0.01$ ,  $b=0.01$ ,  $c=0.05$ ,  $e=0.01$ ,  $f=0.0005$ ,  $d=0.0001$ ,  $g_\alpha=0.000002$ ,  $g_\beta=0.0008$ . This is the normoxia condition, when the cell functions, beyond the transient, without activating the hypoxia cycle. In panel (c) and (d) the homologous quantities (resp. VEGF<sub>i</sub> and W<sub>a</sub>) are depicted for  $g_\alpha = 0.0017$ , while keeping the other parameters unchanged. A residual quota of VEGF<sub>i</sub> molecules is present, which sustains the hypoxia pathway as described in the main text. Finally, when further increasing  $g_\alpha$  ( $g_\alpha = 0.017$  in panels (e) and (f), respectively referring to the VEGF<sub>i</sub> and W<sub>a</sub> concentrations), the cell dies, no activity being asymptotically detected. Solid lines refer to the integration of the mean-field dynamics (11) - (18), while the associated irregular profiles stand for the corresponding stochastic simulations. For all the plots  $N = 10000$ , the initial number of O<sub>2</sub>, W, W\* and HIF- $\alpha$  is 1000, that of HIF- $\beta$ , VEGF<sub>i</sub>, VEGF<sub>0</sub> and E<sub>i</sub> is equal to 100 and, hence, the initial number of E<sub>0</sub> is 5600.

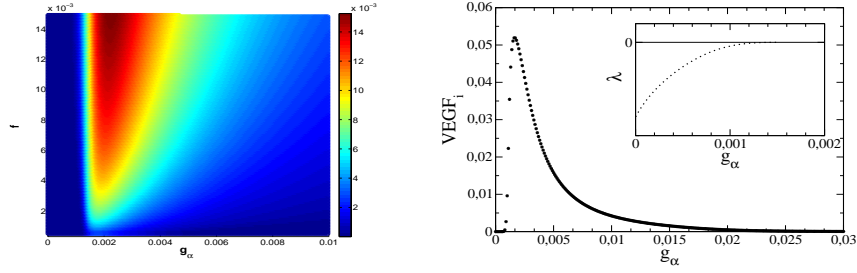


Figure 4: Left panel: The asymptotic concentration of  $\text{VEGF}_i$  is plotted for different values of  $(g_\alpha, f)$ . The data follows from a direct integration of the mean-field Eqs. (11) - (18) and are represented using the colorcode displayed in the legend. Right panel: The concentration of  $\text{VEGF}_i$  is reported as a function of  $g_\alpha$ , for  $f = 0.005$  (the other parameters are set as in Fig. 3). A double transition is clearly displayed, the  $\text{VEGF}_i$  acting as a stabilizer of the cell dynamics for a compact range of  $g_\alpha$  values. Inset a non trivial (see text) real eigenvalue associated to the first family of equilibrium points (normoxia), as a function of  $g_\alpha$ . The eigenvalue is seen to approach zero, i.e. the threshold of stability point, when  $g_\alpha = g_\beta$ . The eigenvalue is calculated via an *ad hoc* semi-analytical procedure which is described in the main body of the paper.

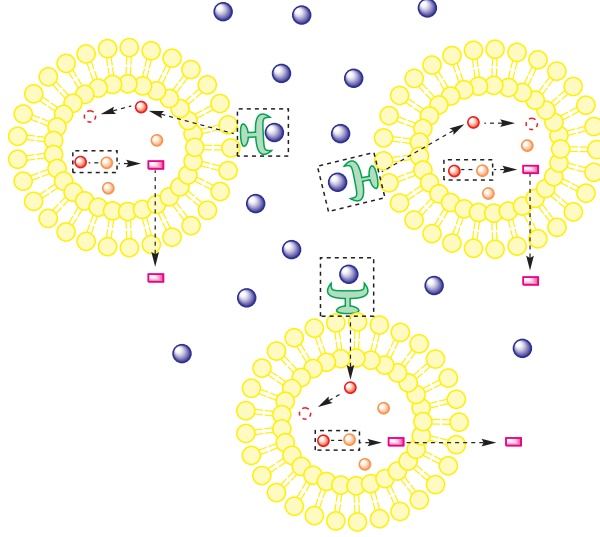


Figure 5: Cartoon of the interaction scheme of three cells. Oxygen molecules (circles laying outside the cells' walls) are now shared, and provides an indirect couplings among the three cells. Each cell is then supporting a whole cycle of internal reactions, as already exemplified in Fig. 1. For the symbols legend, see caption of Fig. 1

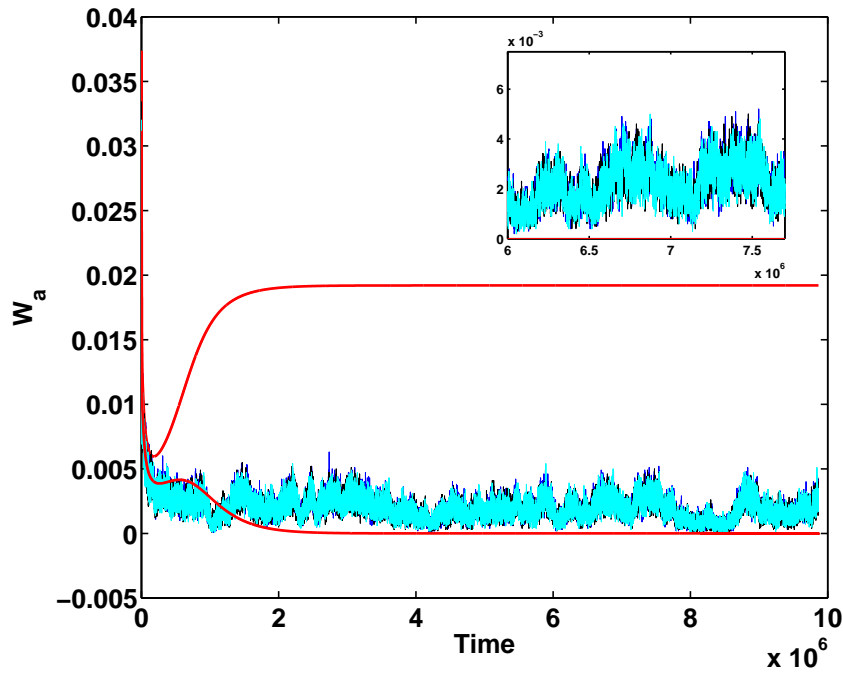


Figure 6:  $W_a$  evolution as a function of time, for a system of three cells, sharing the same oxygen reservoir. The parameters are set so to have two cells in the mean-field region deputed to death, while the third cell is made to function in the hypoxia domain, via a appropriate mutation of the parameter  $g_\alpha$ . All other parameters are identical for the three cells. Solid lines (red online) represent the mean-field dynamics, while the irregular curves (cyan online) stand for the stochastic simulations. Inset: a zoom of the dynamical evolution is represented.

